THE DYNAMIC ASYMMETRIC FRACTURE TEST AND DETERMINATION OF THE DYNAMIC FRACTURE TOUGHNESS OF LARGE-DIAMETER CRACKED ROCK SPECIMENS

by

Yiqiang LU[a], Mingzhong GAO[a, b*], Bin YU[c], Cong LI[a]

[a] State Key Laboratory of Hydraulics and Mountain River Engineering, Sichuan University, Chengdu, China
[b] Institute of Deep Earth Science and Green Energy, Shenzhen University, Shenzhen 518060, China
[c] Datong Coal Mine Group Co. Ltd., Datong 467000, China

We propose large-diameter (160 mm) pre-cracked chevron notched Brazilian disc (P-CCNBD) specimens were used to study the asymmetric fracture law and determine the dynamic fracture toughness of rock. Specimens were diametrically impacted by a split Hopkinson pressure bar. The dynamic fracture failure process of each specimen was monitored by crack propagation gauges and strain gauges. Each of the large-diameter P-CCNBD specimens was found to exhibit prominent asymmetric fracture under impact load. The stress equilibrium condition cannot be satisfied. The dynamic fracture toughness values of the rocks were measured using the experimental-numerical method rather than the quasi-static method. The calculation results showed that the dynamic fracture toughness of rocks increases with the dynamic loading rate. In addition, at the three-dimensional crack front, the dynamic stress intensity factor was found be substantially different at each point. These data suggest that the dynamic fracture toughness of P-CCNBD specimens should be calculated by removing the value affected by an edge arc crack and taking the average value of the remaining points.

Key words: *asymmetric fracture, large-diameter pre-cracked chevron notched brazilian disc (p-ccnbd), dynamic fracture toughness, experimental- numerical method, stress imbalance*

Introduction

During the process of mining solid mineral resources, dynamic fracture problems associated with rock are involved to some degree. In the study of dynamic fracture problems, dynamic fracture toughness, an important dynamic mechanical parameter of rock materials, characterizes the ability of rock to resist crack dynamic initiation and propagation (see [1, 2]).

Currently, Brazilian disc specimens are widely used in split Hopkinson pressure bar (SHPB) systems to evaluate rock dynamic fracture toughness. In 1995, the cracked chevron notched Brazilian disc (CCNBD) was proposed as a specimen for determining rock fracture toughness by the International Society of Rock Mechanics (ISRM) (see [3, 4]). Disc specimens with a diameter below 80 mm have been selected to study rock dynamic fracture toughness by most researchers, such as Zhang et al. [5], Zhou et al. [4] and Dai F et al. [6, 7]. In the dynamic test, stress balance is achieved easily in small specimens, in which condition

*Corresponding author, e-mail: gaomingzhong@163.com

quasi-static methods can be used to determine the dynamic fracture toughness. However, the destruction of rock materials is sensitive to mineral particle size and specimen size. In addition, rock masses in engineering have a larger size. Thus, it is not practical to extend the fracture toughness obtained by small specimens directly to large specimens (see [8-11]). Therefore, it is necessary to study the dynamic fracture failure law of large specimens to understand the large-scale dynamic fracture process in rock engineering. Wang et al. [12] and Yang et al. [13] found that a stress balance could not be achieved in large specimens under a dynamic impact load. However, the asymmetric fracture behavior in specimens caused by stress imbalance was not analyzed in detail. The dynamic asymmetric fracture behavior of large CCNBD specimens containing three-dimensional cracks recommended by ISRM was also not studied.

In view of this background, we perform a dynamic fracture experimental study on large-diameter pre-cracked chevron notched Brazilian disc (P-CCNBD) specimens. The dynamic fracture process of P-CCNBD specimens is monitored by crack propagation gauges (CPGs) and strain gauges (SGs). The dynamic asymmetric fracture law and determination method of the dynamic fracture toughness of large-diameter specimens are studied. The experimental study in this paper is expected to be of great significance for the determination of dynamic fracture toughness using large-diameter rock specimens.

Experimental preparation

Preparation of P-CCNBD specimens

P-CCNBD specimens were obtained by machining two straight cracks in the chevron notch tip of the CCNBD specimen. Because the dynamic propagation behaviors of cracks in a CCNBD specimen under an impact load are complex, the dynamic stress intensity factor (DSIF) time history curve is completely different from that observed with a static load (see [14]), causing the specimen to lose its advantages in the static experiment. Thus, it is not advisable to apply CCNBD static test principles and related data in the dynamic test. In this article, the dynamic fracture toughness of rock is tested by a P-CCNBD specimen containing a prefabricated straight crack. Because of the prefabricated straight crack, the DSIF of the crack tip can be calculated conveniently, and the dynamic fracture toughness of the specimen can be obtained more precisely.

The specimens consisted of gray marble obtained in Nanyang, China. The marble is a fine-grained crystalline structure with homogeneous density and grains sized 0.1-0.3 mm. Its main mineral compositions are calcite, dolomite and wollastonite. The geometrical configuration of the P-CCNBD specimen is shown in Fig. 1. The mechanical parameters and geometrical parameters of the specimens are shown in Table 1.

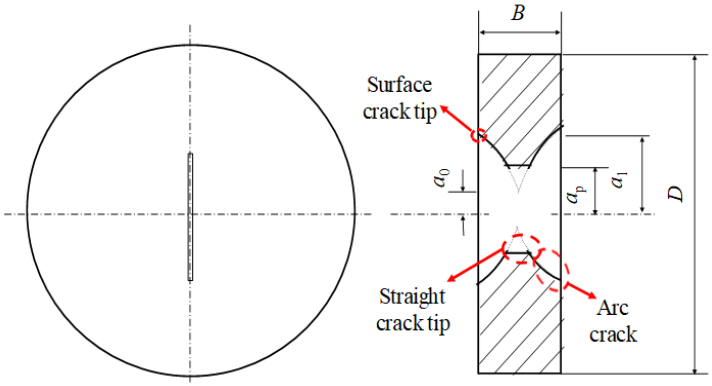

Figure 1. Geometry of specimen P-CCNBD

Table 1. Mechanical parameters and geometrical parameters of the P-CCNBD marble specimens

E/GPa	u	ρ/g·cm^{-3}	c_d/m·s^{-1}	K_{IC}/ MPa·m$^{1/2}$	D/mm	B/mm	a_0/mm	a_1/mm	a_p/mm
69.04	0.26	2.762	5681.1	1.57	160	50	25	46.8	36.5

Loading system and monitoring device

The SHPB loading system was selected in our experiment, as shown in Fig. 2. In the test, the incident bar is impacted by the "shuttle" projectile. This approach can obtain a satisfactory half sine wave and reduce the transverse dispersion effect (see [15]). Hard paper was used as a waveform shaper, and Vaseline was applied to reduce the friction effect of the contact surface of the specimen and the pressure bar.

The CPG crack-monitoring device is shown in Fig. 3. The CPG comprised 10 resistance wires with equal length but different resistors. In the test, the position and timing of the crack was determined according to the mutation position and the time of the voltage signals of the CPG. The CPG device provides advantages in that it has a simple design, high sensitivity, etc. (see, for example, [5, 12]). The parameters for the SHPB and CPG monitoring devices are shown in Table 2.

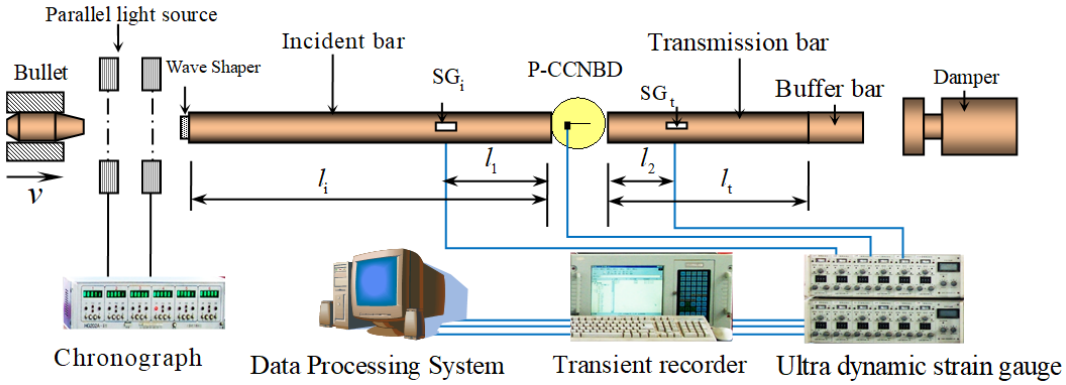

Figure 2. Schematic of the SHPB configuration

Table 2. Parameters for the SHPB and CPG monitoring devices

Material parameter values of the SHPB						Parameters for the CPG monitoring devices [12]			
E_b/GPa	u_b	ρ_b/kg·m^{-3}	C_b/m·s^{-1}	l_i/mm	l_t/mm	CPG resistance/Ω	C.V. source/V	R_{C1}/Ω	R_{C2}/Ω
210	0.3	7850	5244	4500	2500	2	20	1076	50

The crack tips of the P-CCNBD specimen constituted three-dimensional configurations, as shown in Fig. 1. We used SGs 1-4 on the outer surface of the specimen to monitor the cracking signal of the internal crack and two CPGs to monitor the asymmetric fracture process of the surface crack. The positions of attachment of the CPGs and SGs are shown in Fig. 4.

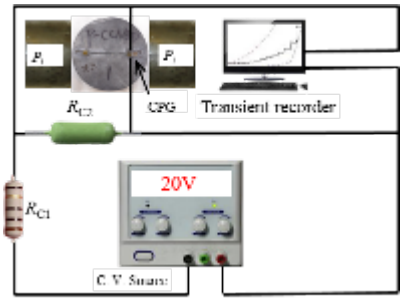

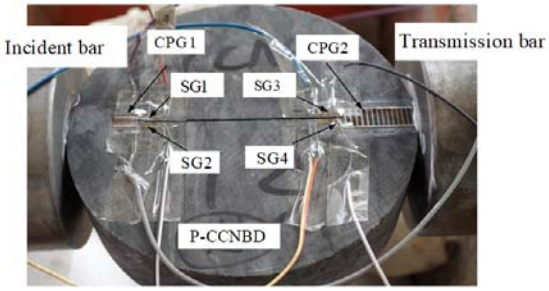

Figure 3. Circuit diagram of the CPG

Figure 4. Positions of attachment of the CPGs and SGs

Experimental recording and data reduction

Dynamic loads on the specimen

As shown in Fig. 2, the signals of the incident wave ε_i and reflected wave ε_r are measured by the strain gauge SG_i, and the transmission wave ε_t signals are recorded by strain gauge SG_t. The strain signals on the incident bar and the transmission bar of specimen M03 are shown in Fig. 5.

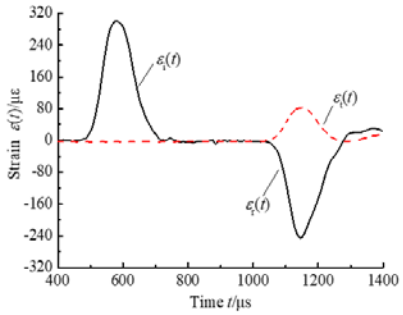

Figure 5. Strain signals of the incident bar and the transmission bar

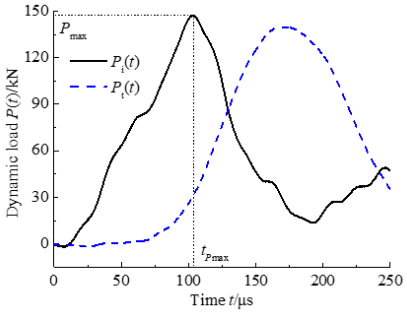

Figure 6. Dynamic forces for loading specimen M03

During the experimental process, the time period of interest occurs after the specimen is loaded on the incident end. The instant when the stress wave first arrives at the incident end is set as zero time. Based on one-dimensional elastic stress wave theory, the loading history curve of the P-CCNBD specimen at the incident end and the transmitted end are determined by Eq. (1a) and Eq. (1b).

$$P_i(t) = E_b A_b [\varepsilon_i(t) + \varepsilon_r(t)] \tag{1a}$$

$$P_t(t) = E_b A_b \varepsilon_t(t) \tag{1b}$$

where E_b and A_b are the elastic modulus and cross-sectional area of the SHPB, respectively.

Fig. 6 shows the dynamic impact load history curve of the specimen M03 at both ends based on Eq. (1). Fig. 6 shows that the maximum load and its corresponding time are P_{max} = 147.16 kN and t_{max} = 102.88 μs, respectively.

Asymmetric fracture process of the P-CCNBD specimen

The voltage signals recorded by the CPG1 and SG1 are plotted in Fig. 7. The time t_{SG1}, which corresponds to the first strain peak of SG1, is taken as the initiation moment of the internal crack tip of the specimen, and the time t_{CPG1}, which corresponds to the first resistance mutation time of the CPG1, is taken as the initiation moment of the surface crack tip of the specimen. t_{SG1} is taken as the crack initiation time of the sample. When the crack tip starts to fracture, unloading occurs, and this reduces the strain recorded by SG1, resulting in a peak, as shown in Fig. 7, similar to the results of Jiang et al. [16]. To accurately obtain the asymmetric fracture process of P-CCNBD specimen, the derivative of the voltage signal of CPG1 and CPG2 is obtained, as shown in Fig. 8.

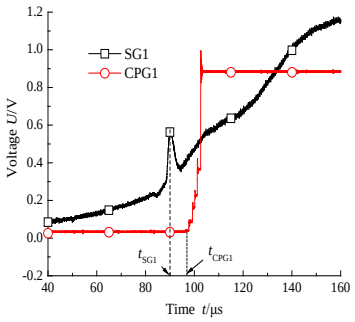

Figure 7. SG1 and CPG1 voltage signals of specimen M03

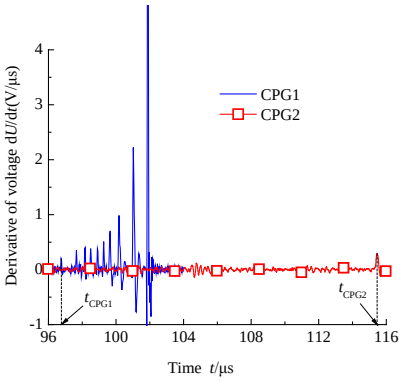

Figure 8. Derivative of the CPG1 and CPG2 voltages

The crack initiation time of CPG1 on specimen M03 is 14.825 μs, which is earlier than that of CPG2. Additionally, before CPG2 is initiated, the crack propagation on the CPG1 path is completed. The results show that the large-diameter P-CCNBD specimen unequivocally follows an asymmetric fracture law under dynamic load. The crack initiation time of 8 specimens at both ends is shown in Table 3.

Table 3 Initiation time of P-CCNBD specimens

Specimen number	P_{max}/kN	t_{Pmax}/μs	t_{CPG1}/μs	t_{SG1}/μs	t_{CPG2}/μs	Δt/μs
M01	138.94	117.68	109.625	102.125	120.900	11.275
M02	130.72	132.48	115.325	110.025	128.300	12.975
M03	147.16	102.88	96.300	90.275	111.125	14.825
M04	146.51	109.10	111.525	105.25	123.750	11.225
M05	168.70	104.75	110.500	103.700	123.225	12.725
M06	133.92	104.10	96.750	91.620	111.075	14.325
M07	168.47	97.78	101.800	94.500	115.800	14.000
M08	146.84	105.99	103.750	97.050	115.250	11. 500

The inertia effect in large specimens cannot be neglected under dynamic loads. The inertia effect leads to asymmetry in the stress distribution on the two crack tips of the specimen at the same moment, and the initiation time of the two crack tips is clearly inconsistent. The distance between the two crack tips of the large-diameter P-CCNBD specimen is $2a_p$ in this article, and the interval of the stress wave reaching the two crack tips is $2a_p/c_d \approx 12.8$ μs, which is essentially consistent with the interval of the two crack tips obtained by the CPGs, as shown in Table 3. Because of the long interval, the two crack initiations are not considered to occur at the same time in the fracture toughness test. Therefore, we recommend that when the dynamic fracture toughness of rock is determined using a large-diameter specimen, the location and time of the first fracture must be determined first to avoid the influence of asymmetric crack initiation on the fracture toughness test value.

Fig. 7 shows that the initiation time t_{SG1} of specimen M03 is 90.275 μs. At this time, the times of stress wave reflection in the specimen are only $(c_d \bullet t_{SG1})/(2D) \approx 1.6$. However, the consensus is that the stress waves can typically reach the stress balance after reflecting 3-5 times back and forth in the specimen (see [17, 18]). Clearly, the basic assumption of testing rock dynamic fracture toughness by the quasi-static method is not satisfied. Therefore, an experimental-numerical method is proposed to determine the dynamic fracture toughness of rock in the article (see [12]), which does not need to satisfy the conditions of quasi-static stress

equilibrium necessarily.

Determination of dynamic fracture toughness

Three-dimensional model of the P-CCNBD specimen

According to the symmetry of the P-CCNBD specimen, the 1/4 three-dimensional model of disk specimen is established by the finite element software ANSYS; 33,422 units and 90,847 nodes are created in the model, as shown in Fig. 9(d). The models are meshed with SOLID95 units. The crack tip is divided by SOLID95 singular units, as shown in Fig. 9(a); the three-dimensional crack tip coordinate system is shown in Fig. 9(b). In the three-dimensional crack tip finite element model of P-CCNBD specimen, many layers of precast straight crack parts exist. To conveniently analyze the variation rule of the DSIF of a straight crack, we establish a local coordinate system along the center of the straight crack (thickness z = 0) and divide the mesh of the straight crack segments into 18 parts, as shown in Fig. 9(c).

The dynamic load $P_i(t)$ obtained by Eq. (1a) is applied to the specimen. The DSIF of the P-CCNBD specimen is calculated by Eq. (2) using the displacement method given in Ref. [19].

$$K_I(t) = \frac{\sqrt{2\pi}E}{24(1-\mu^2)} \frac{8v_B(t) - v_A(t)}{\sqrt{r_{0B}}} \tag{2}$$

where E and μ are the elastic modulus and Poisson's ratio, respectively, r_{0B} is a quarter length of r_{0A} in the singular element, $v_A(t)$ is the time history of the displacement of node An in the vertical (y) direction, and $v_B(t)$ corresponds to node B, as shown in Fig. 9(b).

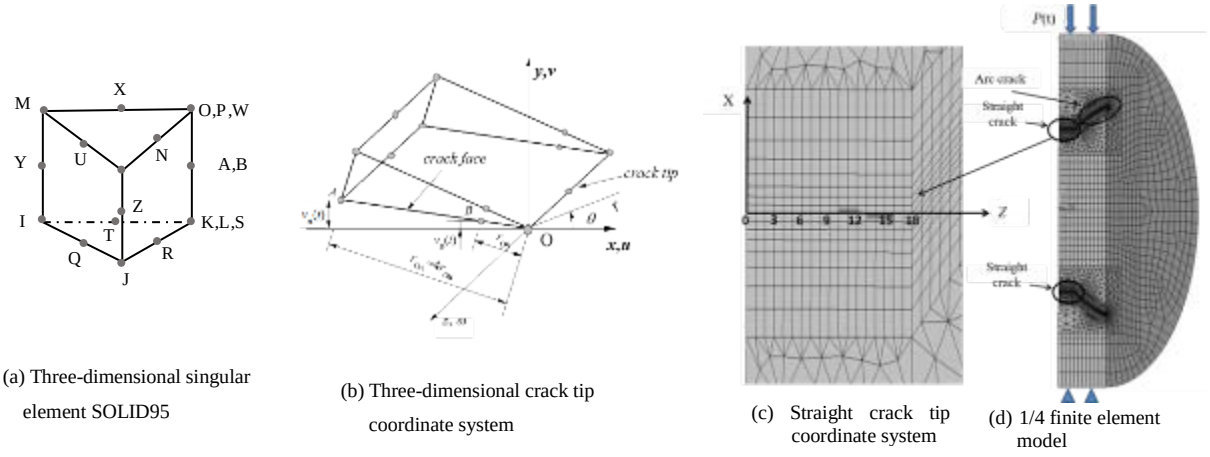

(a) Three-dimensional singular element SOLID95

(b) Three-dimensional crack tip coordinate system

(c) Straight crack tip coordinate system

(d) 1/4 finite element model

Figure 9. One-quarter finite element model of P-CCNBD

Determination of dynamic fracture toughness

According to the finite element model shown in Fig. 9(c), the DSIF time history curves for each node of the incident straight crack are calculated, as shown in Fig. 10. Fig. 10 shows that the curves obtained in each layer node start with a small segment at 0 because it takes some time for the stress wave to arrive the crack tip. Subsequently, as the load gradually increases, the opening displacement generated by the crack tip also gradually increases. When the opening displacement reaches a critical value, the specimen begins to crack. At this time, the DSIF is the dynamic fracture toughness of the specimen, which is denoted by K_{ID}. For specimen M03, at the moment of fracture $t = t_{SG1}$, the DSIF values at each layer of nodes are shown in Fig. 11 with the dimensionless Z/0.5B coordinates.

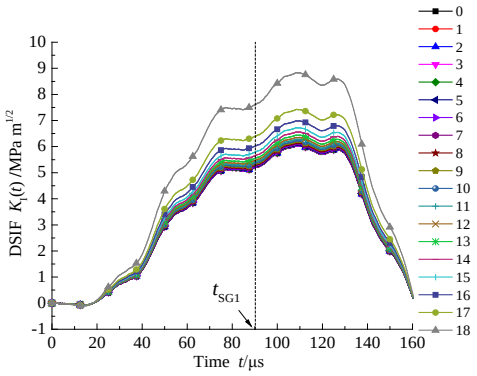

Figure 10. DSIF near the incident bar

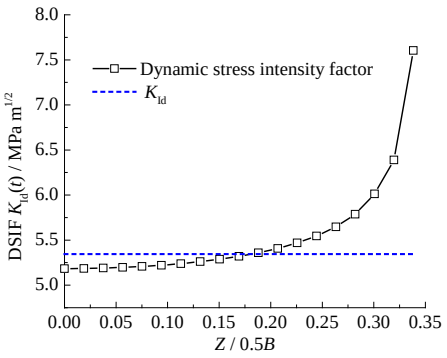

Figure 11. Determination of DSIF and dynamic fracture toughness

As shown in Fig. 11, as the dimensionless z/0.5B coordinates increase, the DSIF gradually increases, and the final 4 values are larger due to the influence of the edge arc crack. To eliminate the influence of the edge arc crack on the fracture toughness value, it is suggested to remove the points in the large range of the edge arc crack and take the average value of the remaining data points as the dynamic fracture toughness of the specimen, similar to Wang Q Z et al.'s [19] method for recalibrating the fracture toughness of a static CCNBD. In this article, the values with dimensionless straight crack lengths in the range of 0.26 to 0.34 are removed, and the average value with dimensionless straight cracks in the range of 0 to 0.26 is used as the dynamic fracture toughness value of the specimen. The dynamic crack fracture toughness values of the P-CCNBD specimens measured by the experimental-numerical method are listed in Table 4.

Table 4 Dynamic fracture toughness obtained with the experimental-numerical method

Specimen number	K_{ID}/MPa·m$^{1/2}$	K_{ID}/K_{IC}	$\dot{K}$ /MPa·m$^{1/2}$·s^{-1}
M01	6.84	4.36	6.698
M02	5.09	3.24	4.626
M03	5.34	3.40	5.915
M04	5.66	3.61	6.109
M05	6.54	4.17	6.307
M06	4.99	3.18	5.446
M07	4.68	2.98	4.952
M08	6.96	4.43	7.172

Influence of loading rate on dynamic fracture toughness

Dynamic fracture tests must take into account the effect of dynamic loading rates on dynamic fracture toughness. The dynamic loading rate K is defined in Eq. (3) using the value given in Ref. [20], and the calculated result for the dynamic loading rate is given in Table 4. Table 4 shows that in the P-CCNBD dynamic test, the loading rate increases from 4.426×10^4 MPa·m$^{1/2}$ s^{-1} to 7.172×10^4 MPa·m$^{1/2}$ s^{-1}, and the corresponding dynamic fracture toughness of 4.68 MPa·m$^{1/2}$ increases to 6.96 MPa·m$^{1/2}$. The results are compared with the research results of scholars working in the same area (Zhang et al. [21], Yang et al. [13], Wang et al. [12], and Zhang et al. [5]). To eliminate the influence of the material properties of the rock, the experimental results are treated dimensionlessly using Eq. (3), and the experimental results are plotted in Fig. 12.

$$\dot{K} = \frac{K_{\mathrm{ID}}}{t_{\mathrm{SG1}}} \tag{3}$$

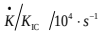

Figure 12. Relation between the dynamic fracture toughness and dynamic loading rate

Fig. 12 shows that the dynamic fracture toughness of both marble and sandstone increases with increasing loading rate and satisfies an approximately linear relationship in the interval from 10^4 to 2×10^5 s^{-1}. However, the rate of increase in the dynamic initiation toughness of different rock materials varies significantly. The dynamic fracture toughness of sandstone and marble summarized in this paper shows that the rate of increase of the dynamic fracture toughness of marble is significantly higher than that of sandstone. The dynamic fracture toughness is related to the physical properties of rock, such as the mineral composition, structural structure, density, and degree of weathering.

Conclusion

In our work, using the SHPB device to impact P-CCNBD marble disc specimens, we found that the crack tip initiation time near the incident bar was generally earlier than the crack tip initiation time near transmission. The large-diameter disc specimens with prefabricated cracks were found to exhibit prominent asymmetric cracking phenomena under impact loading. When a large-diameter disc specimen is used to determine the rock fracture toughness, we recommend that the experimental-numerical method should be used to determine the dynamic fracture toughness and that the dynamic fracture toughness of a crack near the incident bar should be calculated as a test value. In addition, the DSIF of the P-CCNBD specimen gradually increased along the center of the crack tip outward. We recommend that the fracture toughness should be calculated by removing the value of the edge affected by the side arc and taking the average value of the remaining values. The work in this paper provides new ideas and methods for testing rock fracture toughness in large-diameter specimens and addresses the insufficiency of the CCNBD specimen for testing dynamic fracture toughness.

Acknowledgement

This work was financially supported by the State Key Research Development Program of China (Grant No. 2016YFC0600701), National Natural Science Foundation of China (Grant No. 51822403，51674170).

Nomenclature

E, E_{b} - Young’s modulus of marble and SHPB

l_{i}, l_{t} - length of incident and transmission bar

respectively, **[**MPa**]**

u, u_b - Poisson's ratio marble and SHPB respectively

ρ, ρ_b - density of marble and SHPB respectively, **[**kg m^{-3}**]**

c_d, c_b - dilatational wave of marble and SHPB respectively, **[**m s^{-1}**]**

B - thickness of P-CCNBD, **[**mm**]**

$\dot{K}$ - dynamic loading rate, **[**MPa·$m^{1/2}$·s^{-1}**]**

K_{IC} - static fracture toughness, **[**MPa·$m^{1/2}$**]**

CPG - crack propagation gauge

SG - strain gauge

respectively, **[**mm**]**

P_{max} - peak load, [kN]

P_i, P_t - force on the incident and transmission bar–specimen interface respectively, [kN]

D, D_b - diameter of P-CCNBD andSHPB respectively, **[**mm**]**

t_{Pmax} - the time corresponding to the peak load [μs]

t_{CPG1}, t_{CPG2}, t_{SG1} - initiation time of CPG1, CPG2, SG1 respectively, [μs]

K_{ID} - dynamic fracture toughness, [MPa·$m^{1/2}$**]**

P-CCNBD - pre-Cracked Chevron Notched Brazilian Disc

DSIF - dynamic stress intensity factor

References

[1] Freund L B. *Dynamic Fracture Mechanics*, World Publishing Corp, 1991

[2] Zhang Q B, Zhao J., A Review of Dynamic Experimental Techniques and Mechanical Behavior of Rock Materials, *Rock Mechanics & Rock Engineering, 47*(2014), 4, pp. 1411-1478

[3] Fowell R J. Suggested Method for Determining Mode I Fracture Toughness Using Cracked Chevron Notched Brazilian Disc (CCNBD) Specimens, *International Journal of Rock Mechanics and Mining Sciences and Geomechanics Abstracts, 32*(1995), 1, pp. 57-64

[4] Zhou Y X., *et al., Suggested Methods for Determining the Dynamic Strength Parameters and Mode-I Fracture Toughness of Rock Materials*, Springer International Publishing, 2011, pp. 35-44

[5] Zhang Q B, Zhao J., Effect of Loading Rate on Fracture Toughness and Failure Micromechanisms in Marble, *Engineering Fracture Mechanics, 102* (2013), 2, pp. 288-309

[6] Dai F., *et al,*. Determination of Dynamic Rock Mode-I Fracture Parameters Using Cracked Chevron Notched Semi-circular Bend Specimen, *Engineering Fracture Mechanics, 78*(2011),15, pp. 2633-2644

[7] Dai F., *et al.,* Dynamic Cracked Chevron Notched Brazilian Disc Method for Measuring Rock Fracture Parameters, *International Journal of Rock Mechanics & Mining Sciences, 47* (2010), 4, pp. 606-613

[8] Le J L., *et al.,* Subcritical Crack Growth Law and Its Consequences for Lifetime Statistics and Size Effect of Quasibrittle Structures, *Journal of Physics D Applied Physics, 42* (2009), 42, pp. 214008-214015

[9] Bažant Z P., Size Effect in Blunt Fracture, Concrete, Rock, Metal, *Journal of Engineering Mechanics, 110*(1984), 4, pp. 518-535

[10] Qi C., *et al.,* Mechanism Underlying Dynamic Size Effect on Rock Mass Strength, *International Journal of Impact Engineering, 68*(2014), 3, pp. 1-7

[11] Ayatollahi M R, Akbardoost J., Size and Geometry Effects on Rock Fracture Toughness, Mode I Fracture, *Rock Mechanics & Rock Engineering, 47* (2014), 2 , pp. 677-687

[12] Wang Q Z., *et al.,* Sequential Determination of Dynamic Initiation and Propagation Toughness of Rock Using an Experimental–numerical–analytical Method, *Engineering Fracture Mechanics, 14*1(2015), pp. 78-94

[13] Yang J., *et al.,* A New Method for Determining Dynamic Fracture Toughness of Rock Using SCDC Specimens, *Chinese Journal of Rock Mechanics & Engineering, 34*(2015), 2, pp. 279-292

[14] Man K, Zhou H., Research on Dynamic Fracture Toughness and Tensile Strength of Rock at Different Depths, *Chinese Journal of Rock Mechanics and Engineering, 29*(2010), 8, pp. 1657-1663

[15] Zhou Z., *et al.,* Stress Uniformity of Split Hopkinson Pressure Bar under Half-sine Wave Loads, *International Journal of Rock Mechanics and Mining Sciences,* 48 (2011), 4, pp. 697-701

[16] Jiang F., *et al.,* Evaluation of Dynamic Fracture Toughness by Hopkinson Pressure Bar Loaded Instrumented Charpy Impact Test, *Engineering Fracture Mechanics, 71* (2004), 3, pp. 279-287

[17] Jiang F, Vecchio K S., Hopkinson Bar Loaded Fracture Experimental Technique, A Critical Review of Dynamic Fracture Toughness Tests, *Applied Mechanics Reviews, 62* (2009), 6, pp. 1469-1474

[18] Zhang S., *et al.,* Influence of Different Dynamic Load Calculating Methods on Rock Dynamic Fracture Toughness Test, *Chinese rock and Soil Mechanics, 34* (2013),9, pp. 2721-2726

[19] Wang Q Z., *et al.,* Recalibration and Clarification of the Formula Applied to the ISRM-Suggested CCNBD Specimens for Testing Rock Fracture Toughness, *Rock Mechanics & Rock Engineering, 46* (2013), 2, pp. 303-313

[20] Li Z L, Wang Q Z., Experimental Research on Effect of Loading Rate for Dynamic Fracture Toughness of Rock, *Chinese Journal of Geotechnical Engineering,* 28 (2006), 12, pp. 2116-2120

[21] Zhang C., *et al.,* Determination of Dynamic Fracture Initiation, Propagation, and Arrest Toughness of Rock Using SCDC Specimen, *Chinese Journal of Theoretical and Applied Mechanics, 48* (2016), 3, pp. 624-635

Paper submitted: March 12, 2018
Paper revised: July 11, 2018
Paper accepted: December15, 2018